Enhancing stochastic multi-microgrid operational flexibility with mobile energy storage system and power transaction

Z.L. Qu, J.J. Chen *, K. Peng, Y.L. Zhao, Z.K. Rong, M.Y. Zhang

School of Electrical and Electronic Engineering, Shandong University of Technology, Zibo, 255000, China

A R T I C L E I N F O	A B S T R A C T
	With the increased uncertainty and variability of net load induced from high penetrations of renewable energy, independent operation of single microgrid (MG) is facing great operational problems such as high operation cost, low self-consumption of local renewable energy and exacerbating peak and valley load. In this paper, a mobile energy storage system (MESS) and power transaction-based flexibility enhancement strategy is proposed for interconnecting multi-microgrid (MMG) considering uncertain renewable generation. The MESS can move between different microgrids by a truck, and we use this temporal–spatial flexibility to provide charging/discharging service for MMG. Then, the Aumann–Shapley is developed for expenses allocating in MMG system with MESS and power transaction due to ensuring the fairness and reasonableness is of the utmost important in collaborative operation. After that, the expected power not served (EPNS) and expected power curtailment (EPC) are derived as the risk measure to evaluate the uncertain renewable energy from the perspective of risk aversion. Numerical studies show that MESS for MMG operation enables the reduction in total operational cost of diesel generator by 23.58%, the improvement in total grid connection volumes of wind and solar by 7.17%, and the improvement in smoothness of the total load curve by 0.92%. Besides, interconnected system for MMG operation enables the improvement in total grid connection volumes of wind and solar by 6.69%, and the improvement in smoothness of the total load curve by 1.50% in comparison with the unconnected system.

1. Introduction

With the rapid development of industrial technologies, traditional fossil fuels are facing a huge depletion crisis, which has promoted the utilization of renewable energy to gradually increase to meet human energy demand (Das et al., 2021). At present, renewable energy is delivered to the grid mainly through centralized or distributed methods (Ruan et al., 2020). The distributed integration of renewable energy method is conducive to promoting the local use of renewable energy and the reliability of power supply in comparison with centralized integration, which has caused extensive research by scholars (Al-Ghussain et al., 2020). As an effective utilization mode of distributed renewable energy, microgrid (MG) is a new subject studied by domestic and international researchers in recent years (Atia & Yamada, 2016). About 34% of global MG projects are in the United States, providing the experience to other countries in policy, control systems, and demonstration projects (Feng et al., 2018). Besides the United States, MG projects in the Asia-Pacific region are also growing rapidly, which accounts for about 40% of the global MG capacity. Japan's New Energy and Industrial Technology Development Organization (NEDO) has provided

funding for MG research, which is mainly related to new energy solutions, power supply reliability, and flexible electrical control (Ustun et al., 2011). Three representative renewable energy island MGs have been built and are operating in the East China Sea to provide green and reliable electricity supply (Zhao et al., 2018). In summary, many countries are developing MG projects in the world.

Wind and solar resources are one of the most competitive sources of renewable energy (Liu et al., 2019). After the large-scale integration of wind and solar resources into the power grid, the problem of insufficient flexibility of the MG system is outstanding because of the inherent volatility and randomness (Elkadeem et al., 2020). The MG system thus needs to have greater flexibility to cope with the defects of wind and solar resources. If the flexibility of the system is insufficient, to ensure the safety and stability of the power system, it is necessary to properly curtail wind and solar or shed load when the load demand is too small or too large (Croce et al., 2020). However, the curtailment of wind and solar is contrary to the original intention of developing renewable energy, while load shedding will cause greater economic

---

losses. Therefore, the higher flexibility of the MG system has greater significance for the large-scale integration of wind and solar resources.

On the one hand, for the interconnected multi-microgrid (MMG) system, multiple adjacent MGs constitute an interconnected and mutually-powered MMG system in a certain area, which can decrease the operating cost of system (Wang et al., 2019). For example, Zhang et al. (2018) formulated the problem of transaction coordination and economic operation of MMG as a unit commitment optimization problem to minimize the operational cost. Wu et al. (2012) adopted co-ordinated information and strategies among MMG based on the autonomous control model to decrease the operating cost of distributed generation. And Li et al. (2018) proposed an interconnected scheduling model for energy and reserve, using distributed energy storage to optimize the operation of MMG system. On the other hand, mobile energy storage system (MESS) is mobilized by a big truck and connected to the distribution system at different stations in comparison with stationary energy storage system (SESS). And MESS is one of the most effective way to reduce operating cost and enhance resilience in distribution systems. For example, Abdeltawab and Mohamed (2017) presented a day-ahead energy management system based on MESS to reduce the cost of grid power supply. Lei et al. (2016) introduced the potential of MESS in enhancing the resilience of distribution systems to cope with extreme weather, which not only can improve the ability of power supply systems to withstand critical loads, but also improve the ability to recover after disasters. Similarly, the two-stage optimization model was proposed in Kim and Dvorkin (2018), with the goal of improving the resilience of distribution systems through MESS and MGs.

From existing literature we notice that: (i) Prior work is rarely mentioned in interconnected MMG system and MESS working together to improve flexibility, especially to reduce the daily MMG operating cost, improve penetration level of wind and solar power as well as smooth load profile. (ii) Ignoring the uncertainty of wind and solar resources may lead to MMG operational solutions becoming infeasible by the analyst (Li et al., 2017). (iii) If MMG operational flexibility with MESS and power transaction is considered, the proper allocation of economic cost to each MG needs to be studied, as it should undertake corresponding cost when the MG exists power transaction or MESS provides charging/discharging service for the MG.

For addressing above issues, enhancing stochastic MMG operational flexibility with MESS and power transaction is studied. The main contributions of this paper are shown as follows:

(1) MESS and power transaction-based flexibility enhancement strategy for MMG system is studied, which aims to reduce the daily MMG operating cost, improve penetration level of wind and solar power as well as smooth load profile.

(2) EPNS and EPC-based risk assessment (RA) is devised for uncertain wind and solar power. The RA needs neither to sample a large number of wind and solar power, nor to calculate a complex multi-objective optimization problem.

(3) The value of Aumann–Shapley is used for allocating economic cost of MMG system. And the effectiveness of the proposed model is verified by evolutionary predator and prey strategy (EPPS) algorithm.

2. Configuration of mobile energy storage system

2.1. Temporal–spatial characteristics of MESS

The transportation network is modeled by the temporal–spatial characteristics, which has been widely applied to optimize the problem of vehicle routing and scheduling (Yao et al., 2019). Therefore, the temporal–spatial characteristics of MESS among MMG is presented, as shown in Fig. 1, and it is constituted by MG stations and trip arcs, showing all possible transportation routes. Two types of trip arcs are defined in the temporal–spatial characteristics of MESS as follows. *(1) Moving arcs:* it connects two different MG stations and represents a movement both time and spatial locations. For example, as shown in

Fig. 1, the MESS can move from MG 1 to MG 2 or MG 3 during the transit time interval. *(2) Holding arcs:* it connects two same MG stations, and it indicates that MESS is not moving during the dispatch period. This means that the MESS continues to provide charging/discharging service for the MG. The entire transportation paths of MESS can be represented by continuous trip arcs, which indicates the departure MG station and destination MG station.

For the sake of illustrating the dynamic location information of MESS, we define the binary variables $u_n(t) \in \{0, 1\}$, which represents the state of MESS at time t. $u_n(t) = 1$ if the MESS locates at MG station n at time t, and $u_n(t) = 0$ if the MESS does not locate at MG station n at time t.

$\zeta_{n,m}(t)$ is the transportation time between MG stations n and m at time t, which is constituted of three segments: traffic congestion delay $k_{\text{tra}}(t)$, commute time $D_{n,m}/v_{\text{MESS}}$ and installation time $\epsilon_{\text{MESS}}^{\text{ins}}$ (Abdeltawab & Mohamed, 2017).

$$\zeta_{n,m}(t) = \begin{cases} \text{round}\left(\frac{k_{\text{tra}}(t) + D_{n,m}/v_{\text{MESS}} + \epsilon_{\text{MESS}}^{\text{ins}}}{\Delta T_{\text{h}}} \right), n \neq m \\ 0, n = m \end{cases} \quad (1)$$

where $n, m = 1, 2, \ldots, N_{\text{MG}}$, and N_{MG} is the number of MG. $D_{n,m}$ represents the transportation distance between MG stations n and m at time t, v_{MESS} is the average moving speed of MESS, and $k_{\text{tra}}(t)$ is a time-dependent index that gives an indicator of the traffic delay at time t. ΔT_{h} is the unit time step in hour.

Since $\zeta_{n,m}(t)$ denotes the transportation time between MG stations n and m at time t, the MESS departing from MG station n at time t cannot be connected to MG station m until time $t + \zeta_{n,m}(t)$. This can be summarized as:

$$u_n(t) + \frac{1}{N_{\text{MG}} \cdot \Gamma} \sum_{0 \leq \delta_{n,m}(t) \leq \zeta_{n,m}(t)} \sum_{m \neq n} u_m\left(t + \delta_{n,m}(t)\right) \leq 1, \quad \forall n, \forall m \quad (2)$$

$$\Gamma = \max_{n,m,t} \left\{ \zeta_{n,m}(t) \right\}, \quad \forall n, \forall m, \forall t \quad (3)$$

where $\delta_{n,m}(t) \in \left\{0, 1, \ldots, \zeta_{n,m}(t)\right\}$, and Γ is the maximum value of $\zeta_{n,m}(t)$ for all cases of n, m at time t.

According to (2) and (3), the transit-time decomposition matrix Q is developed considering transit model of MESS, and the detailed descriptions please refer to Kwon et al. (2019).

$$Q = \begin{bmatrix} \mathbf{I} & \mathbf{Y}_1^1 & \mathbf{Y}_2^1 & \cdots & \mathbf{Y}_\Gamma^1 & \mathbf{O} & \mathbf{O} & \cdots & \mathbf{O} \\ \mathbf{O} & \mathbf{I} & \mathbf{Y}_1^2 & \mathbf{Y}_2^2 & \cdots & \mathbf{Y}_\Gamma^2 & \mathbf{O} & \cdots & \mathbf{O} \\ \vdots & \vdots & \vdots & \vdots & \vdots & \vdots & \vdots & \vdots & \vdots \\ \mathbf{O} & \mathbf{O} & \mathbf{O} & \mathbf{O} & \mathbf{O} & \cdots & \mathbf{O} & \mathbf{I} & \mathbf{Y}_1^{\text{T}-1} \end{bmatrix} \quad (4)$$

where

$$\mathbf{Y}_\tau^t = \frac{1}{N_{\text{MG}} \cdot \Gamma} \begin{bmatrix} 0 & y_{\tau 12}^t & \cdots & y_{\tau 1 N_{\text{MG}}}^t \\ y_{\tau 21}^t & 0 & \cdots & y_{\tau 2 N_{\text{MG}}}^t \\ \vdots & \vdots & y_{\tau nm}^t & \vdots \\ y_{\tau N_{\text{MG}} 1}^t & y_{\tau N_{\text{MG}} 2}^t & \cdots & 0 \end{bmatrix},$$

$$\forall \tau \in \left\{0, 1, \ldots, \zeta_{n,m}(t) \ldots, \Gamma\right\} \quad (5)$$

$$y_{\tau nm}^t \in \{0, 1\}, \quad \forall n, \forall m, \forall t, 0 \leq \tau \leq \Gamma \quad (6)$$

In (4), $\mathbf{I}$ is the identity matrix, $\mathbf{O}$ is the zero matrix, and T is the number of scheduling intervals in a day. In (5), $y_{\tau nm}^t$ is a binary constant. $y_{\tau nm}^t = 1$ for $0 \leq \tau \leq \zeta_{n,m}(t)$, indicating that MESS can arrive at MG station m at time $t + \zeta_{n,m}(t) + 1$; otherwise, $y_{\tau nm}^t$ is set to 0.

2.2. Operation constraints of MESS

When arrives at a MG, the MESS provides charging/discharging service for the MG, while satisfying the following operation constraints:
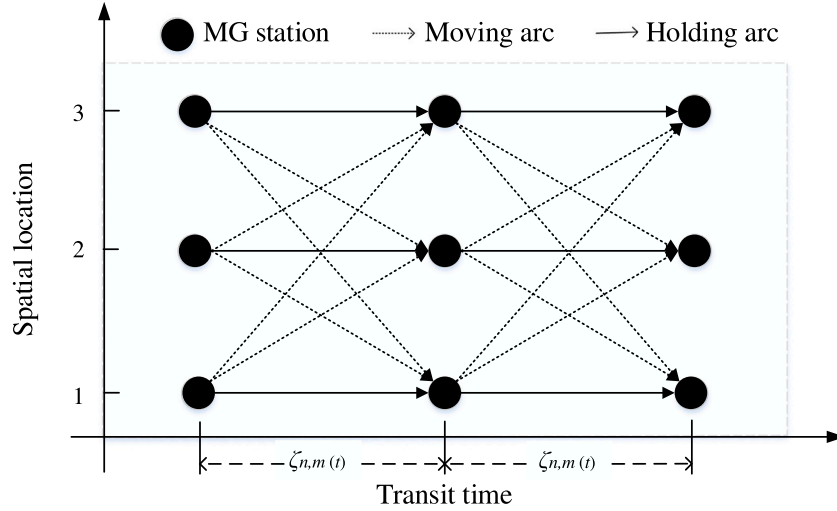
Fig. 1. Temporal–spatial characteristics of MESS.

$$
(7) \begin{cases}
SOE(0) = SOE(T) & \text{(a)} \\
SOC(t) = \dfrac{SOE(t)}{E_{\text{MESS}}} & \text{(b)} \\
E_{\text{MESS}} = \dfrac{SOE_{\max} - SOE_{\min}}{SOC_{\max} - SOC_{\min}} & \text{(c)} \\
SOE(t) = SOE(t-1) + (1 - \gamma(t)) P_{\text{MESS}}^{\text{ch},t} \eta_{\text{MESS}}^{\text{ch}} + \dfrac{\gamma(t) P_{\text{MESS}}^{\text{dch},t}}{\eta_{\text{MESS}}^{\text{dch}}} & \text{(d)}
\end{cases}
$$

where state of energy (SOE) is used to describe the estimation of the available energy state of MESS, satisfying (7).(a) (7)(b) represents state of charge (SOC), and it is the ratio of available power to the maximum available capacity of the MESS, E_{MESS} represents the maximum available capacity of the MESS calculated by (7)(c). $SOC_{\min}$ and $SOC_{\max}$ are respectively the minimum and maximum SOC of MESS. $SOE_{\min}$ and $SOE_{\max}$ are respectively the minimum and maximum SOE of MESS. For $\forall t \in (0, T)$, the mathematical model between the SOE and the charging/discharging power can be expressed as (7)d), where $P_{\text{MESS}}^{\text{ch/dch},t}$ and $\eta_{\text{MESS}}^{\text{ch/dch}}$ represent charging/discharging power and efficiency of MESS, respectively (Zheng et al., 2018). The binary variables $\gamma(t) \in \{0, 1\}$ are defined to represent the charging/discharging state of MESS at time t, let $\gamma(t) = 1$ denotes that the MESS is in the discharging state at the MG station, and $\gamma(t) = 0$ denotes that the MESS is in the charging state at the MG station.

3. Problem formulation

Microgrid is defined as a decentralized group of loads and distributed energy resources that normally operates connected to and synchronous with the main grid, but can also disconnected to "island state" and operation autonomously. Microgrid can improve the reliability of supply by changing between connected and island model, and it can effectively integrate renewable energy (Cagnano et al., 2020). Fig. 2 shows the structure of the studied three-microgrid system in a radial feeder, where each MG consists of one wind turbine (WT), one photovoltaic (PV), one diesel generator (DG) and local load demand. In the system, MESS is a large energy storage battery with a truck as a carrier, and it can be inserted into different MG stations during different time intervals for providing charging/discharging service. In addition, the power transaction among different MGs is also considered in the MMG system to address the issues of power surplus or shortage of MG. The goal of this paper is to take the advantages of the transportability and interconnection to reduce the daily MMG operating cost, improve penetration level of wind and solar power, and last but not least, smooth load profile.

3.1. Objective function

The objective function of MESS based flexibility improvement for MMG scheduling under uncertain environment aims to minimize the total economic cost (EC). In EC, it consists of the operational cost (OC) of DG and MESS, the transaction cost (TC) of selling/purchasing power with the other MGs and DPN, and EPNS and EPC costs of wind and solar power, which is shown as follows:

$$
C = \sum_{n=1}^{N_{\text{MG}}} \sum_{t=1}^{T} \left(a_{\text{DG}}^n P_{\text{DG}}^{n,t} + b_{\text{DG}}^n \right) \tag{8a}
$$

$$
+ \sum_{n=1, m \neq n}^{N_{\text{MG}}} \sum_{t=1}^{T} \left(e_{\text{MG}}^t \left(P_{\text{MG,B}}^{n,m,t} - P_{\text{MG,S}}^{n,m,t} \right) + e_{\text{DPN}}^t \left(P_{\text{DPN,B}}^{n,t} - P_{\text{DPN,S}}^{n,t} \right) \right) \tag{8b}
$$

$$
+ \sum_{n=1}^{N_{\text{MG}}} \sum_{t=1}^{T} \left(u_n(t) e_{\text{MESS}} | P_{\text{MESS}}^{\text{ch/dch},t} | \right) + \sum_{t=1}^{T} \left(\rho_{\text{MESS}} | P_{\text{MESS}}^{\text{ch/dch},t} | \right) + C_{\text{labor}} \tag{8c}
$$

$$
+ \sum_{n=1}^{N_{\text{MG}}} \sum_{t=1}^{T} \left(e_{\text{DPN}}^t P_{\text{WT,EPNS}}^{n,t} + \lambda P_{\text{WT,EPC}}^{n,t} \right) \tag{8d}
$$

$$
+ \sum_{n=1}^{N_{\text{MG}}} \sum_{t=1}^{T} \left(e_{\text{DPN}}^t P_{\text{PV,EPNS}}^{n,t} + \lambda P_{\text{PV,EPC}}^{n,t} \right) \tag{8e}
$$

where (8a) represents OC of DG, a_{DG}^n and b_{DG}^n are the OC coefficients, and $P_{\text{DG}}^{n,t}$ stands for output of DG in the nth MG at time t. (8b) represents TC of exchange power including electricity purchased/sold among MGs and DPN. $P_{\text{MG,B}}^{n,t}$ and $P_{\text{MG,S}}^{n,t}$ are respectively the exchange power among MGs, and e_{MG}^t is the electricity price of power transaction in different MGs at time t. Similarly, $P_{\text{DPN,B}}^{n,t}$ and $P_{\text{DPN,S}}^{n,t}$ are respectively the exchange power between MG and DPN, and e_{DPN}^t is the electricity price of power transaction between MG and DPN at time t. (8c) models the OC of MESS. e_{MESS} and $P_{\text{MESS}}^{\text{ch/dch},t}$ denote the cost coefficients and charging/discharging power of MESS at time t, respectively. ρ_{MESS} is a given degradation cost coefficient of MESS. And C_{labor} is the truck labor cost which includes the daily allowance of the truck driver and technical staff. (8d) and (8e) denote the EPNS and EPC costs after wind and solar power integration, and λ denotes EPC penalty coefficient.

3.2. Constraints

In order to ensure the safety and reliability of the system within the allowed power limits, the optimal solution must meet the following constraints.

(1) Generation constraints: In order to obtain optimal MMG scheduling solutions, WT, PV, DG and MESS are constrained by their technical
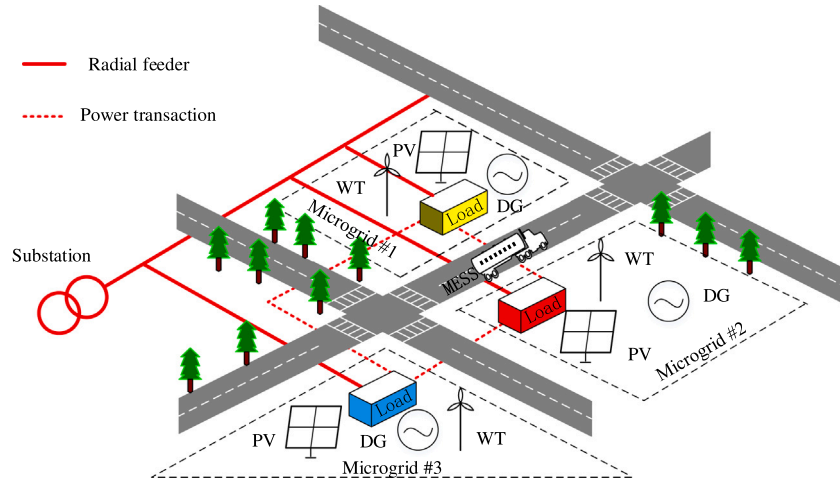
Fig. 2. Typical structure of a three-microgrid system with MESS and power transaction.

limits as follows:

$$P_{\text{WT,min}}^n \leqslant P_{\text{WT}}^{n,t} \leqslant P_{\text{WT,max}}^n \tag{9}$$

$$P_{\text{PV,min}}^n \leqslant P_{\text{PV}}^{n,t} \leqslant P_{\text{PV,max}}^n \tag{10}$$

$$P_{\text{DG,min}}^n \leq P_{\text{DG}}^{n,t} \leq P_{\text{DG,max}}^n \tag{11}$$

$$- R_{\text{down}}^n \leq P_{\text{DG}}^{n,t} - P_{\text{DG}}^{n,t-1} \leq R_{\text{up}}^n \tag{12}$$

$$\left| P_{\text{MESS}}^{\text{ch/dch},t} \right| \leq P_{\text{MESS,max}}^{\text{ch/dch}} \tag{13}$$

$$SOC_{\min} < SOC(t) < SOC_{\max} \tag{14}$$

where constraints (9)–(11) ensure that WT, PV and DG satisfy the upper and lower power generation limits in each MG at time t. $P_{\text{WT,min}}^n$, $P_{\text{PV,min}}^n$ and $P_{\text{DG,min}}^n$ are respectively minimum outputs of WT, PV and DG in the nth MG. $P_{\text{WT,max}}^n$, $P_{\text{PV,max}}^n$ and $P_{\text{DG,max}}^n$ are respectively maximum outputs of WT, PV and DG in the nth MG. Constraint (12) means that the output of DG should satisfy the ramp up and down rate limits during the adjacent time intervals. R_{up}^n and R_{down}^n are respectively maximum ramp up and down rates of DG in the nth MG. Eq. (13) defines the MESS charging/discharging power limit. $P_{\text{MESS,max}}^{\text{ch/dch}}$ is maximum charging/discharging power of MESS. Finally, Eq. (14) denotes the SOC upper and lower limits of MESS (Paul et al., 2019).

(2) Exchange status constraints: Each MG is designed to purchase/sell electricity from the other MGs, or purchase/sell electricity from DPN. But purchasing and selling electricity cannot be simultaneously for each MG at time t. Therefore, the power exchange status of each MG is denoted by binary variables:

$$r_{n,m}(t) + s_{n,m}(t) \leqslant 1, \quad \forall n, m \in N_{\text{MG}}, \quad m \neq n, \forall t \in T \tag{15}$$

$$v_n(t) + w_n(t) \leqslant 1, \quad \forall n \in N_{\text{MG}}, \quad \forall t \in T \tag{16}$$

where $r_{n,m}(t)$ and $s_{n,m}(t)$ are exchange status among MGs. There is no power transaction between MGs n and m when $r_{n,m}(t) = s_{n,m}(t) = 0$ at time t. Else, either $r_{n,m}(t)$ or $s_{n,m}(t)$ equals to 1, there exists power transaction among MGs. In this case, $r_{n,m}(t) = 1$ if MG n purchases power from MG m at time t, and $s_{n,m}(t) = 1$ if MG n sells power to MG m at time t. $v_n(t)$ and $w_n(t)$ are exchange status between MG and DPN. Likewise, there is no power transaction between MG n and DPN when $v_n(t) = w_n(t) = 0$ at time t. Else, either $v_n(t)$ or $w_n(t)$ equals to 1, there exists power transaction between MG and DPN. In this case, $v_n(t) = 1$ if MG n purchases power from DPN at time t, and $w_n(t) = 1$ if MG n sells power to DPN at time t.

(3) Exchange power constraints: Considering technical limits of transmission lines and inverter, exchange power should satisfy the following constraints:

$$0 \leqslant P_{\text{MG,B}}^{n,m,t} \leqslant r_{n,m}(t) P_{\text{MG,max}}^{n,m}, \quad \forall n, m \in N_{\text{MG}}, \quad m \neq n, \quad \forall t \in T \tag{17}$$

$$0 \leqslant P_{\text{MG,S}}^{n,m,t} \leqslant s_{n,m}(t) P_{\text{MG,max}}^{n,m}, \quad \forall n, m \in N_{\text{MG}}, \quad m \neq n, \quad \forall t \in T \tag{18}$$

$$0 \leqslant P_{\text{DPN,B}}^{n,t} \leqslant v_n(t) P_{\text{DPN,max}}^n, \quad \forall n \in N_{\text{MG}}, \quad \forall t \in T \tag{19}$$

$$0 \leqslant P_{\text{DPN,S}}^{n,t} \leqslant w_n(t) P_{\text{DPN,max}}^n, \quad \forall n \in N_{\text{MG}}, \quad \forall t \in T \tag{20}$$

$$P_{\text{MG,B}}^{n,m,t} = P_{\text{MG,S}}^{m,n,t}, \quad \forall n, m \in N_{\text{MG}}, \quad m \neq n, \quad \forall t \in T \tag{21}$$

where $P_{\text{MG,B}}^{n,m,t}$, $P_{\text{MG,S}}^{n,m,t}$, $P_{\text{DPN,B}}^{n,t}$ and $P_{\text{DPN,S}}^{n,t}$ denote power purchased from other MGs, power sold to other MGs, power purchased from DPN and power sold to DPN at time t, respectively (Cui et al., 2019).

(4) Load balance constraint: The sum of outputs of WT, PV and DG, charging/discharging power of MESS and the transaction power must meet the local load demand $P_{\text{L}}^{n,t}$ of each MG at time t:

$$P_{\text{DG}}^{n,t} + P_{\text{WT}}^{n,t} + P_{\text{PV}}^{n,t} + P_{\text{MG,B}}^{n,m,t} + P_{\text{DPN,B}}^{n,t} = P_{\text{L}}^{n,t} + P_{\text{MESS}}^{\text{ch/dch},t} + P_{\text{MG,S}}^{n,m,t} + P_{\text{DPN,S}}^{n,t} \tag{22}$$

3.3. EPNS and EPC-based RA for uncertain wind and solar power

In order to acquire reliable MMG scheduling solutions under the fluctuation and forecasting uncertainty of wind and solar power, this paper converts uncertain wind and solar power into confidence interval variables, and proposes EPNS and EPC-based RA for evaluating uncertain wind and solar power. The model regards EPNS and EPC as risk measure to evaluate the potential loss of load due to WT and PV generation uncertainty. At the same time, the model does not need to sample a large number of wind and solar power to simulate the true distribution or calculate a complex multi-objective optimization problems to account for the feasibility of wind and solar power generation (Chen et al., 2017). The detailed descriptions of risk measure are given as below.

The confidence interval of wind and solar power under a given confidence level is explained in Chen et al. (2017). Thus, we take wind power as an example and consider 95% confidence level of wind power, then $\alpha = 0.05$, $Z_{1-\frac{\alpha}{2}} = 1.96$, and the confidence interval of wind power is

$$\frac{P_{\text{WT}}^{n,t} - \mu^t}{\sigma^t} \in [-Z_{1-\frac{\alpha}{2}}, Z_{1-\frac{\alpha}{2}}] \Rightarrow P_{\text{WT}}^{n,t} \in [\mu^t - Z_{1-\frac{\alpha}{2}} \sigma^t, \mu^t + Z_{1-\frac{\alpha}{2}} \sigma^t]$$
$$\Rightarrow P_{\text{WT}}^{n,t} \in [\mu^t - 1.96\sigma^t, \mu^t + 1.96\sigma^t] \tag{23}$$

where μ^t and σ^t are the mean value and standard deviation of wind power at time t, respectively.

According to the characteristics that the wind power $P_{\text{WT}}^{n,t}$ follows Gaussian distribution in a short term, the probability density function $f\left(P_{\text{WT}}^{n,t}\right)$ and cumulative distribution function $F(P_{\text{WT}}^{n,t})$ of wind power
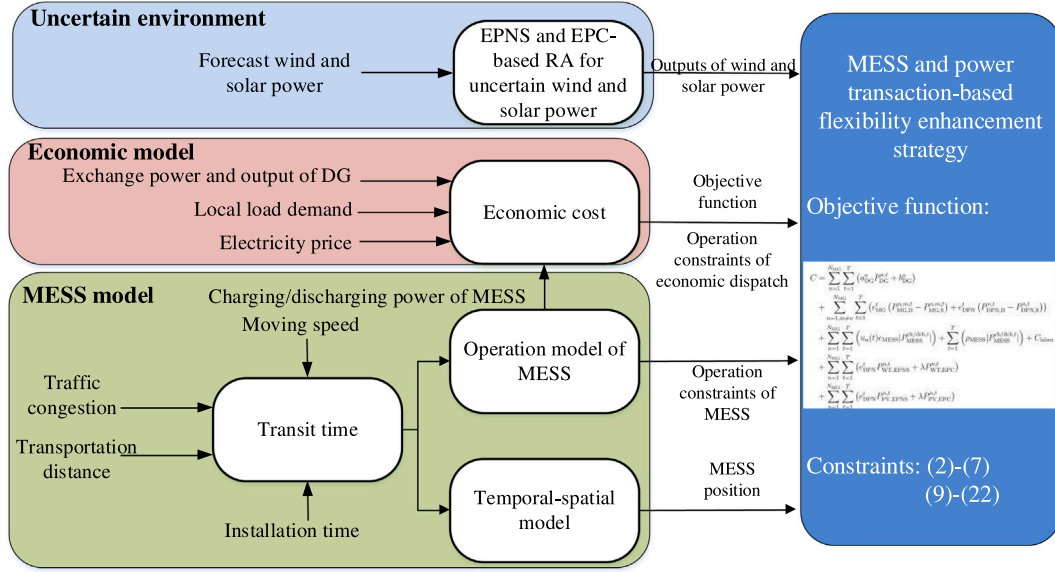
Fig. 3. The flow chart of stochastic MMG scheduling with MESS and power transaction.

are given as follows (Li et al., 2014):

$$f\left(P_{\mathrm{WT}}^{n,t}\right) = \frac{1}{\sigma^t \sqrt{2\pi}} e^{-\frac{\left(P_{\mathrm{WT}}^{n,t}-\mu^t\right)^2}{2\left(\sigma^t\right)^2}} \tag{24}$$

$$F(P_{\mathrm{WT}}^{n,t}) = \frac{1}{\sigma^t \sqrt{2\pi}} \int_0^{P_{\mathrm{WT}}^{n,t}} e^{-\frac{(x-\mu^t)^2}{2\left(\sigma^t\right)^2}} \, dx \tag{25}$$

Thus the hourly EPNS of wind power in the nth MG $P_{\mathrm{WT,EPNS}}^{n,t}$ is given by

$$P_{\mathrm{WT,EPNS}}^{n,t} = \int_{P_{\mathrm{WT,min}}^{n}}^{P_{\mathrm{WT}}^{n,t}} \left(P_{\mathrm{WT}}^{n,t} - x\right) f(x) dx \tag{26}$$

and the hourly EPC of wind power in the nth MG $P_{\mathrm{WT,EPC}}^{n,t}$ is described by

$$P_{\mathrm{WT,EPC}}^{n,t} = \int_{P_{\mathrm{WT}}^{n,t}}^{P_{\mathrm{WT,max}}^{n}} \left(x - P_{\mathrm{WT}}^{n,t}\right) f(x) dx \tag{27}$$

Similarly, according to the probability density function $f\left(P_{\mathrm{PV}}^{n,t}\right)$ and cumulative distribution function $F(P_{\mathrm{PV}}^{n,t})$ of solar power (Ran et al., 2015), the hourly EPNS $P_{\mathrm{PV,EPNS}}^{n,t}$ and EPC $P_{\mathrm{PV,EPC}}^{n,t}$ of solar power in the nth MG are given by Eqs. (28) and (29), respectively. .

$$P_{\mathrm{PV,EPNS}}^{n,t} = \int_{P_{\mathrm{PV,min}}^{n}}^{P_{\mathrm{PV}}^{n,t}} \left(P_{\mathrm{PV}}^{n,t} - x\right) f(x) dx \tag{28}$$

$$P_{\mathrm{PV,EPC}}^{n,t} = \int_{P_{\mathrm{PV}}^{n,t}}^{P_{\mathrm{PV,max}}^{n}} \left(x - P_{\mathrm{PV}}^{n,t}\right) f(x) dx \tag{29}$$

4. Research method

The flow chart of stochastic MMG scheduling with MESS and power transaction is shown in Fig. 3, and the topology of the MMG system is depicted in Fig. 4. The main steps for the scheduling are listed as follows.

Step 1: Set up EPPS algorithm parameters: group scale, the maximum number of calculations, and bounds of the variables.

Step 2: Input forecast values of wind power, solar power, load demand and electricity price. And then input device parameters of WT, PV and DG.

Step 3: Input traffic congestion, moving speed, transportation distance and installation time of MESS. And obtain temporal–spatial characteristics of MESS according to (1)–(6).

Step 4: Calculate the objective function C by EPPS algorithm under constraints (7) and (9)–(29). And obtain the OC of DG and MESS, the TC of selling/purchasing power with the other MGs and DPN, and EPNS and EPC costs of wind and solar power.

Step 5: Determine outputs of WT, PV and DG, exchange power among MGs, and position and charging/discharging power of MESS.

5. Aumann–Shapley and evolutionary predator and prey strategy algorithm

Shapley value is one of the important classical solutions in cooperative games, and it reflects the average marginal contribution of members to each sub-alliance. However, the computational complexity of the Shapley value increases exponentially with the increase in the number of participating members, and the allocation results are easily affected by the relative size of the participating members and lack of fairness (Amaris et al., 2018).

The Aumann–Shapley value method is an extension of the Shapley value theory in an infinite number of in-game alliances. It can solve the problem of income distribution in an infinite number of in-games through limiting treatment and analysis. The basic idea is to divide each player into an infinite number of players, and then use Shapley method to calculate the allocation of each small player (Faria et al., 2009). The essence of Aumann–Shapley value method is to find the average value of the marginal contribution of each player to each cooperative alliance. Therefore, the impact of the order in which each player joins the alliance on the allocation results can be ignored. It has economic consistency and equality, and can achieve fair and reasonable allocation. The Aumann–Shapley value method has been widely used in power system congestion cost allocation, transmission cost allocation, and network loss allocation (Junqueira et al., 2007).

This paper applies the Aumann–Shapley value method to allocate EC of MMG system. The EC allocated to the nth MG based on the Aumann–Shapley value method is the integral of its power from 0 to P^n.

$$\pi_n = \int_0^{P^n} \frac{\partial C\left(\frac{x\boldsymbol{P}}{P^n}\right)}{\partial P^n} \mathrm{d}x = P^n \int_0^1 \frac{\partial C(x\boldsymbol{P})}{\partial P^n} \mathrm{d}x \tag{30}$$
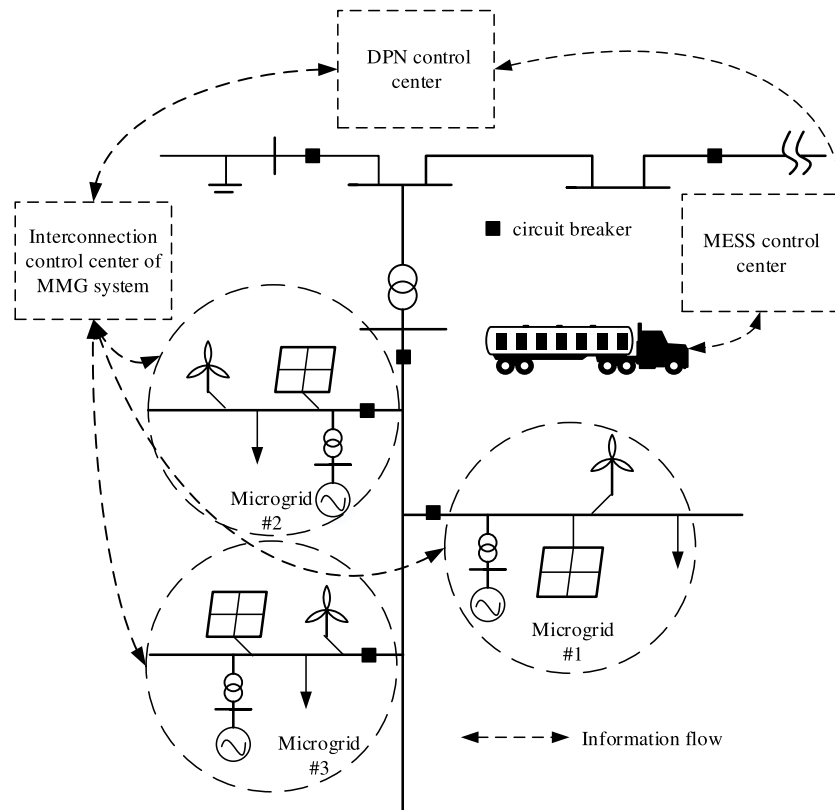
Fig. 4. The topology of the MMG system.

where π_n is EC of the nth MG. $\boldsymbol{P}$ is the power vector of resources of the MMG system including output of DG, charging/discharging power of MESS and exchange power among MGs and DPN. $C(x\boldsymbol{P})$ is the cost function of EC obtained by Eq. (8). $\boldsymbol{P}^n$ is the power vector of resources of the nth MG.

On the other hand, in order to obtain the optimal scheduling solution of the MMG system, this paper adopts a group intelligent optimization algorithm named evolutionary predator and prey strategy (EPPS). This algorithm studied the dynamic interaction behaviors between Australian hunting dogs and goats, including hunting dog predatory behavior and goat escape behavior. And then, the algorithm proposes the concepts of empirical predator, strategic predator, prey and safe location to simulate the predator-escape behavior between the two animals: hunting dog predator mechanism, goat scanning mechanism and goat escape mechanism. In EPPS, the experience predator refers to the hounds that directly prey on goats, the strategic predator refers to the hounds that can adjust the predation path through the exchange of population information, the prey refers to the goats chased by the hounds, and the safe position refers to the refuge that the chased goat needs to seek. Based on these concepts, EPPS uses animal scanning strategies, predation strategies and escape strategies to design evolutionary algorithms.

In EPPS, the individual with the best fitness value in each generation is selected as the prey, and the individual with the worst fitness value in each generation is selected as the safe location. In addition to prey and safe locations, the remaining individuals are randomly divided into experience predators and strategic predators. EPPS studied three processes from the perspective of predator predation and prey escape. When a group of predators find prey, the experienced predator will directly pursue the prey based on the experience. They will scan the safe location and try to escape from the predicament when the prey finds itself in a dangerous situation. As for the strategic predators, they will update their predation routes in real time according to the

---

Algorithm 1 The pseudocode of EPPS algorithm

1: Initial group scale $:= Pop$ and set up algorithm parameters;
2: Calculate the objective function value C, store the current individual as the initial solutions, and determine the prey and the safe location according to the best and worst fitness value;
3: Set $g := 0$, the maximum number of iterations $:= Max\_G$, and the index of the prey $:= index^{(0)}$;
4: **while** $g \leq Max\_G$ **do**
5:    Calculate the scanning distance at the gth generation prey $l_{\max}^{(g)}$;
6:    **for** $i = 1 : Pop$ **do**
7:       **if** $i == index^{(g)}$ **then**
8:          Prey perform search mechanism according to the scanning directions and scanning distance;
9:       **else if** $rand < 0.3$ **then**
10:         Experienced predators perform search mechanism based on successful paths of the other predators;
11:       **else**
12:         Strategic predators perform search mechanism based on the preyâĂŹs position and escaping direction;
13:       **end if**
14:    **end for**
15:    Adjust the position of each individual if constraint is satisfied;
16:    Adjust the prey, the safe location and $index$ according to the calculated the fitness value of each individual;
17:    $g = g + 1$;
18: **end while**

---

route where the prey escape. The pseudocode of EPPS is presented in Algorithm 1 and the specific search mechanism of predators and prey is illustrated in Chen et al. (2016).
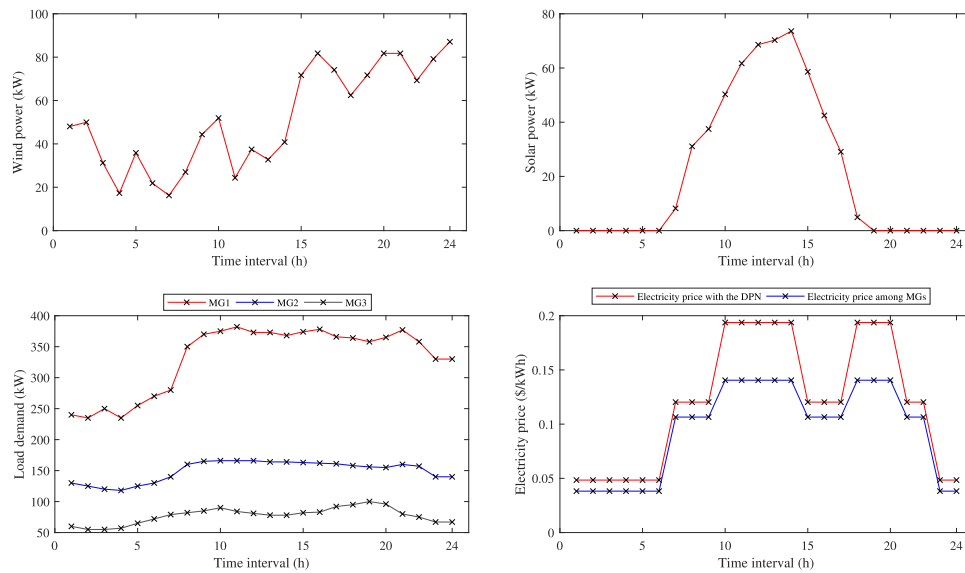
Fig. 5. Forecast values of wind power, solar power, load demand and electricity price.

6. Case study

6.1. Simulation settings

To prove the validity of the proposed model, numerical studies are conducted on a three-microgrid system with MESS. Each MG system is constituted of WT, PV, DG and local load demand, and the corresponding parameter settings of DG are shown in Table 1. The upper limit of exchange power in each transaction is set to 50 kW. In terms of MESS and SESS, the related parameters including charging/discharging efficiency and power, the range of SOC, moving speed and so on, are shown in Table 2. Forecast values of wind power, solar power, load demand and electricity price are shown in Fig. 5, and forecast errors of load demand and electricity price are set to be 10% and 20% (Li et al., 2018), respectively. We adopt EPPS algorithm to solve the MMG scheduling problem, and the sample population and the maximum number of calculation are set to 100 and 100,000, respectively. All the simulation are conducted on a desktop personal computer with a 2.60-GHz Inter Core i7 processor with 16.0 GB of RAM under MATLAB environment.

In order to verify the effectiveness of MESS and power transaction-based flexibility improvement strategy for MMG under uncertain environment, simulation results are analyzed in the following three segments:

(1) The comparison of MESS and interconnected MMG system working together on flexibility enhancement in comparison with SESS and unconnected MMG system.

(2) The comparison of the penetration level of wind and solar power under the proposed model, bi-probability-interval optimization (BPIO) model and conditional value-at-credibility (CVaC) model.

(3) The comparison of PSO, GSO and EPPS in solving the proposed optimization model.

6.2. Simulation results and discussion

6.2.1. Simulation about MESS and SESS on flexibility improvement

Fig. 6 offers the charging/discharging power, the position and SOC of MESS. The histogram represents the charging/discharging power of MESS while the dash and solid lines with marks indicate the locations and SOC of MESS, respectively. Note that a negative power represents discharging state of MESS, while a positive power indicates

the charging state of MESS. As shown in Fig. 6, MESS provides charging/discharging service for MG1 in 05:00–06:00, 07:00–08:00, 14:00–15:00, 18:00–19:00 and 21:00–22:00, MG2 in 01:00–02:00, 03:00–05:00, 08:00–09:00, 11:00–12:00, 13:00–14:00, 15:00–16:00, 19:00–21:00 and 22:00–01:00 and MG3 in 02:00–03:00, 06:00–07:00, 09:00–11:00, 12:00–13:00 and 16:00–18:00. MESS is mainly docked at stations MG2 and MG3. The reason for this phenomenon is that MG2 and MG3 have a higher sharing of wind and solar power with a bigger fluctuation of load curve than that of MG1. MESS thus needs to provide charging/discharging service to mitigate the fluctuation of the net load with high penetrations of wind and solar power. Moreover, the SOC value of MESS mainly fluctuates between 1 and 0.2, as shown in Fig. 6, which satisfies the constraint (14).

For the sake of illustrating the advantages of MESS for flexibility improvement in reducing operation cost and increasing penetration rate of renewable energy, this paper compares two MMG system models. One is a MMG system model using MESS (model 1), and the other is a MMG system model using SESS (model 2). The optimal capacity of MESS is 30kWh, which is much less than that of the SESS. That is, the MESS based energy sharing strategy can reduce investment cost in installing energy storage. The optimal hourly outputs of DG in each MG are provided in Fig. 7, and OC of DG as shown in Table 3. Evidently, we can see that model 1 has less output of DG than model 2. Compared with model 2, the OC of DG in each MG are reduced by 30.57%, 21.42% and 15.21%, respectively. In addition, it can be also observed from Fig. 8 that the optimal outputs of wind and solar power in model 1 are more than these of model 2 in each MG. The penetration rate of wind and solar power of model 1 in each MG is 51.27%, 57.38% and 55.86%, while the penetration rate of wind and solar power of model 2 is 41.26%, 51.35% and 51.57%. By contrast, the grid connection volumes of wind and solar in each MG are increased by 10.01%, 6.03% and 4.29%, respectively. Therefore, the optimization results verify the MESS can improve MMG flexibility in terms of reducing energy storage capacity, saving OC of DG and improving wind and solar power penetration level.

In order to accurately estimate the property of implementing MESS in improving the load curve's characteristics, the parameters of the load factor, peak to valley, and peak compensate are adopted as shown by Eqs. (31)–(33), respectively (Dehnavi & Abdi, 2016). Eq. (31) is used to evaluate the smoothness of the load curve, and the larger its value, the smaller the fluctuation of load demand. It is ideally 100% which shows

Table 1
DG parameters of MMG system.

	a_{DG}^n ($/kW)	b_{DG}^n ($)	R_{up}^n (kW/h)	R_{down}^n (kW/h)	$P_{DG,min}^n$ (kW)	$P_{DG,max}^n$ (kW)
MG1	0.19433	0	80	75	40	200
MG2	0.19455	0	40	35	40	100
MG3	0.19515	0	40	35	40	100

Table 2
MESS and SESS parameters of MMG system.

	η^{ch}/ η^{dch}	SOC_{max}/ SOC_{min}	P_{max}^{ch}/P_{max}^{dch}(kW/h)	v_{MESS}(km/h)	e($/kW)	ρ
MESS	0.9	1/0.2	25/20	20	0.221	0.01
SESS	0.9	1/0.2	25/20	–	0.221	0.01

Table 3
Operational cost of DG for each MG about models 1 and 2.

Hour	MG1		MG2		MG3	
	Model 1 ($)	Model 2 ($)	Model 1 ($)	Model 2 ($)	Model 1 ($)	Model 2 ($)
1	12.0402	19.6159	10.7160	12.8760	11.0946	13.2809
2	15.3429	19.6003	11.2344	13.4443	11.8633	13.7235
3	19.6720	20.9075	10.6455	14.9837	10.2281	12.5849
4	14.4298	22.2292	11.7105	12.7472	11.1999	13.0601
5	13.9366	17.4818	10.3374	14.3551	12.0873	13.5439
6	11.8705	18.9230	10.5512	13.8370	9.1828	13.4645
7	11.8585	22.6506	8.9279	14.1275	10.3097	13.0471
8	11.5319	21.2447	14.2870	14.4275	12.0210	13.3383
9	16.5059	16.9534	12.3438	13.4217	14.1867	14.3928
10	10.0809	21.1837	9.4069	13.2326	11.2096	13.5744
11	9.0544	18.7349	9.7879	13.3741	10.3020	14.0061
12	12.9119	19.5773	9.5913	13.7524	15.4445	15.7064
13	9.9575	18.8041	11.1920	14.3227	11.8243	11.9416
14	15.2785	18.1421	10.5617	13.4198	11.5391	12.6774
15	19.8529	20.3899	8.7917	13.0691	8.9474	11.9421
16	15.7825	18.0922	10.1011	13.0779	10.9206	12.3621
17	19.4759	21.4419	9.2942	14.8007	13.3872	13.8100
18	15.5283	22.5063	13.2063	13.3082	10.9671	12.8299
19	15.0567	22.1218	9.4214	14.1366	12.4811	14.0608
20	14.7591	22.8759	10.8688	13.7745	10.7139	14.4675
21	13.7892	20.7229	10.6402	13.1296	11.6542	13.7902
22	11.7739	19.8684	10.9930	13.1091	10.9895	14.6490
23	13.5433	23.6670	10.4386	12.8564	10.5626	13.5000
24	14.2537	19.5454	11.4926	12.8907	10.5189	12.9866
Total	**338.2873↓**	487.2502	**256.5412↓**	326.4744	**273.6354↓**	322.7399
Drop rate	30.57%	–	21.42%	–	15.21%	–
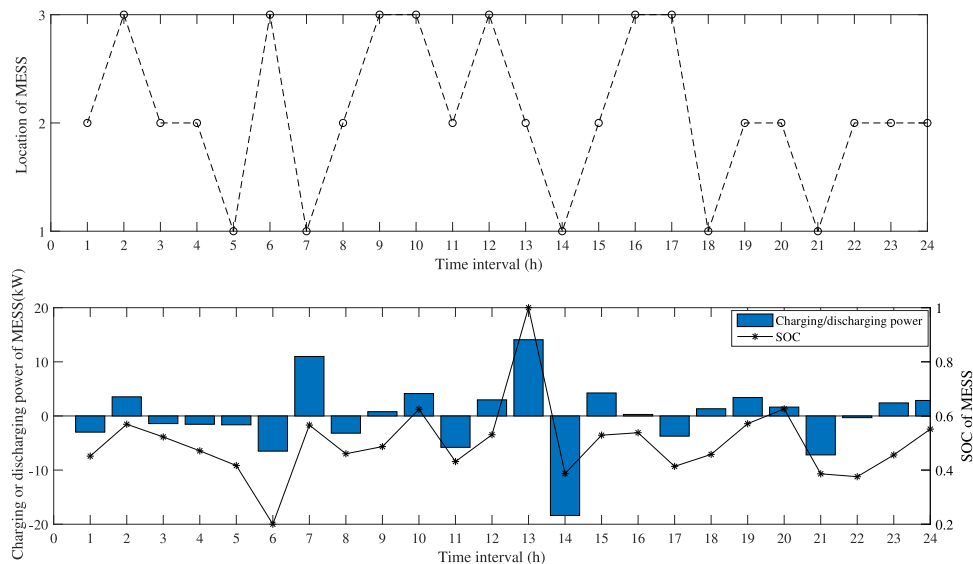
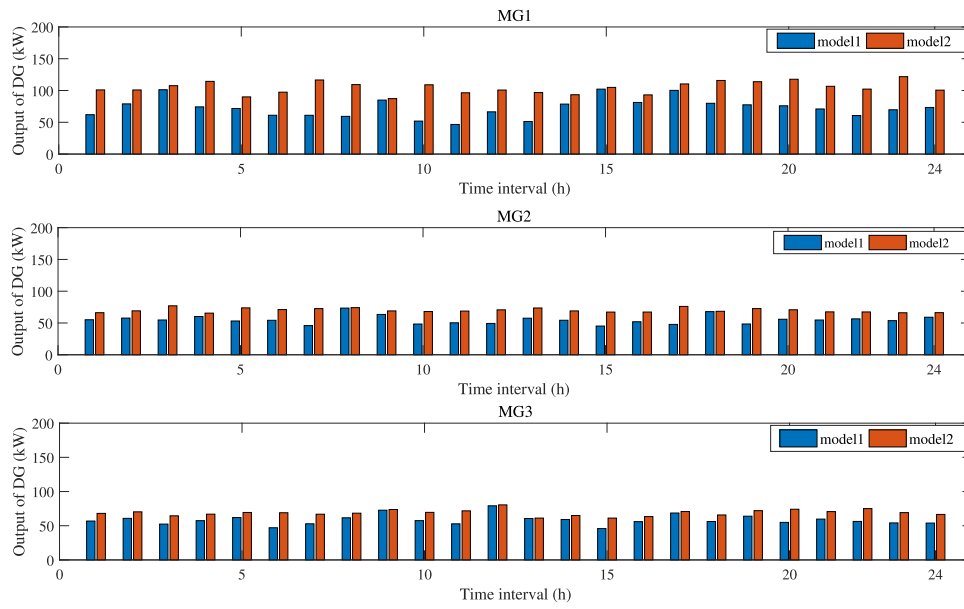**Fig. 6.** Location and charging/discharging power of MESS.

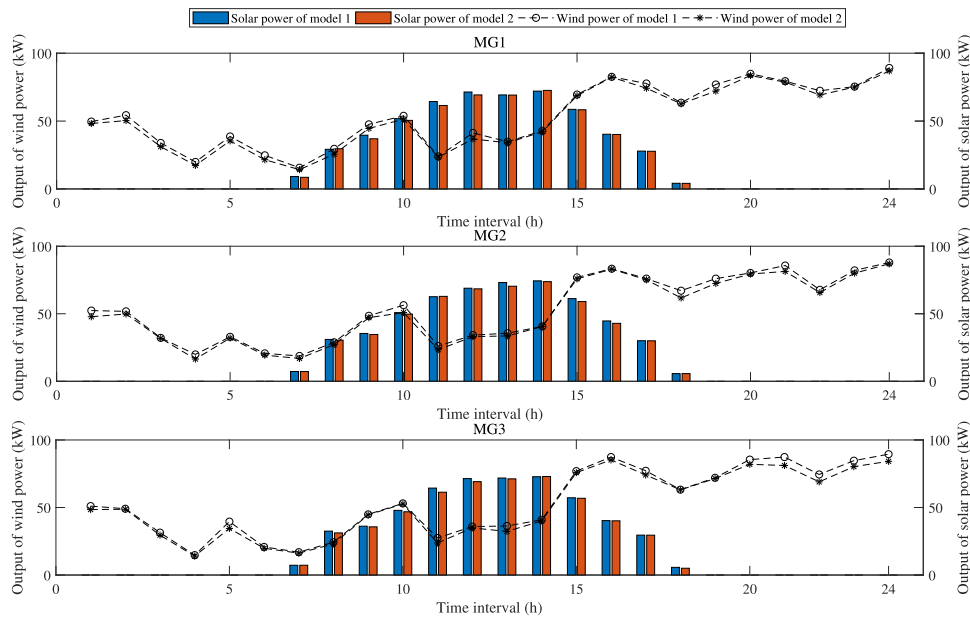**Fig. 7.** Output of DG for each MG about model 1 and 2.

Fig. 8. Outputs of wind and solar power for each MG about model 1 and 2.

Table 4
The characteristics of the load curve about each MG.

Item	MG1			MG2			MG3		
	$F1$	$F2$	$F3$	$F1$	$F2$	$F3$	$F1$	$F2$	$F3$
With WT and PV	71.16%	60.99%	–	62.33%	83.39%	–	6.24%	172.38%	–
MESS, WT and PV	**72.38**% ↑	**59.24**% ↓	1.87%	**63.69**% ↑	**82.19**% ↓	1.51%	**6.50**% ↑	**171.88**% ↓	0.98%

that load demand is constant and does not change with the time.

Peak to valley represents the distance ratio between peak to valley as follows:

$$F1 = Load - factor\% = 100 \times \left(\frac{\sum_{t=1}^{T} P_{L,item}^{n,t}}{T \times \max\{P_{L,item}^{n,t}\}} \right) \quad (31)$$

$$F2 = Peak - to - valley\% = 100 \times \left(\frac{\max\{P_{L,item}^{n,t}\} - \min\{P_{L,item}^{n,t}\}}{\max\{P_{L,item}^{n,t}\}} \right) \quad (32)$$
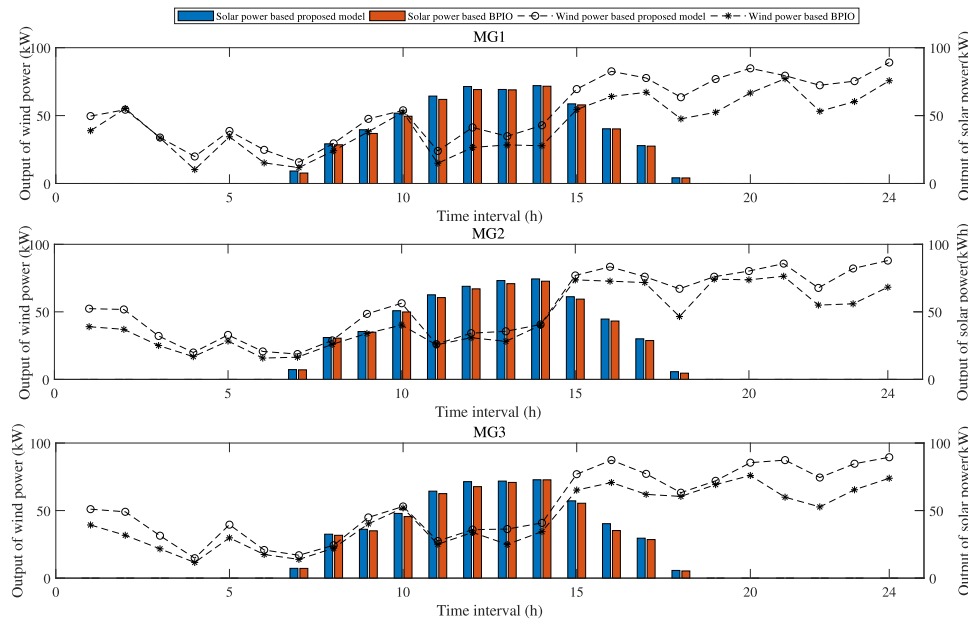
Fig. 9. Outputs of wind and solar power based on the proposed and BPIO model.

Peak compensate shows the normalized amount of peak reduction after implementing MESS and wind and solar grid-connected:

$$F3 = Peak-Compensate\% = 100 \times \left(\frac{\max\{P_{L,WP}^{n,t}\} - \max\{P_{L,MESS}^{n,t}\}}{\max\{P_{L,WP}^{n,t}\}} \right) \quad (33)$$

where $P_{L,item}^{n,t}$ represents the load curve after implementing wind power, solar power and MESS, i.e., $P_{L,WP}^{n,t} = P_L^{n,t} - P_{WT}^{n,t} - P_{PV}^{n,t}$ represents the load curve with wind and solar power, $P_{L,MESS}^{n,t} = P_L^{n,t} - P_{WT}^{n,t} - P_{PV}^{n,t} - P_{MESS}^{ch/dch,t}$ represents the load curve with wind power, solar power and MESS. The above three characteristics of the load curve are explained in Table 4. From the table, the load factor $F1$ increases 1.22%, 1.36%, 0.26% than that without implementing MESS in each MG, and the factor of peak compensate $F3$ increases 1.87%, 1.51%, 0.98%, while the factor of the peak to valley $F2$ decreases 1.75%, 1.2%, 0.5%, respectively. And the reason why the peak to valley $F2$ of MG3 is greater than 100% is that the outputs of wind and solar power exceed the load demand. Therefore, MESS for MMG operation can improve flexibility in smoothing load profile and reducing peak–valley difference.

According to the optimal MMG operational solution for {MG1, MG2, MG3}, we obtain the OC and TC of MMG system, which are calculated by Eq. (30). The above correlative values are shown in Table 5. As seen in Table 5, the OC of DG and TC of power transaction in MG1 are the highest due to the largest load demand. And it can be also observed from Table 5 that MG3 sells power to the other MGs or DPN for economic benefit. This is because the load demand of MG3 is low, and it has redundant power to provide for the other MGs. In addition, the OC of MESS in terms of {MG1}, {MG2} and {MG3} are $35.2624, $72.8466 and $41.6536, respectively. That is, OC of MESS in MG is related to locations and charging/discharging power shown in Fig. 6. Therefore, the proposed EC allocation strategies of MMG system based Aumann–Shapley value has economic consistency and equality, and can achieve fair and reasonable cost allocation.

6.2.2. Simulation about interconnected and unconnected MMG system on flexibility improvement

To investigate the impact of wind and solar power penetration, this subsection conducts numerical experiments with interconnected and unconnected system, and the numerical results are summarized in Table 6. As we can see in Table 6, for each MG, the penetration rate of wind and solar power in the interconnected system increases

Table 5
OC of DG, TC of power transaction and OC of MESS for each MG in {MG1, MG2, MG3}.

MG	OC of DG ($)	TC of power transaction ($)	OC of MESS ($)
MG1	338.2873	514.5249	35.2624
MG2	256.5412	70.9908	72.8466
MG3	273.6354	−162.1765	41.6536
Total	868.4639	423.3392	149.7626

Table 6
Penetration rate of wind and solar power in interconnected and unconnected MMG system.

System type	MG1	MG2	MG3
Interconnected System	51.27%	57.38%	55.86%
Unconnected System	41.67%	52.23%	51.76%

9.60%, 5.15% and 4.10% in comparison with the unconnected system, respectively.

The load curve's characteristics of unconnected and interconnected systems are shown in Table 7. From the table, the load factor $F1$ of interconnected system increases 2.31%, 2.20%, 0.33% than that unconnected system, and the factor of peak compensate $F3$ increases 0.43%, 1.31%, 8.12%, while the factor of the peak to valley $F2$ decreases 2.45%, 10.42%, 16.01%, respectively. The results are understandable because energy can be transmitted among MGs and the interconnected MMG system can cope with volatility and intermittence of wind and solar with more flexibly.

6.2.3. Simulation comparison among different risk evaluation models under uncertain environment

In order to verify the effectiveness of EPNS and EPC-based RA for uncertain wind and solar power, the proposed RA model is compared with BPIO and CVaC model. The core of BPIO model is to obtain the optimal scheduling solution by considering risk and profit of wind and solar power integration. CVaC model is a credibility assessment-based risk aversion model. The optimal hourly outputs of wind and solar power under the proposed model and BPIO are illustrated by Fig. 9. Fig. 10 shows the optimal hourly outputs of wind and solar power under the proposed model and CVaC model. It is observed from two figures that the grid connection volume based on EPNS and EPC-based RA model is higher than that of the BPIO and CVaC model at most
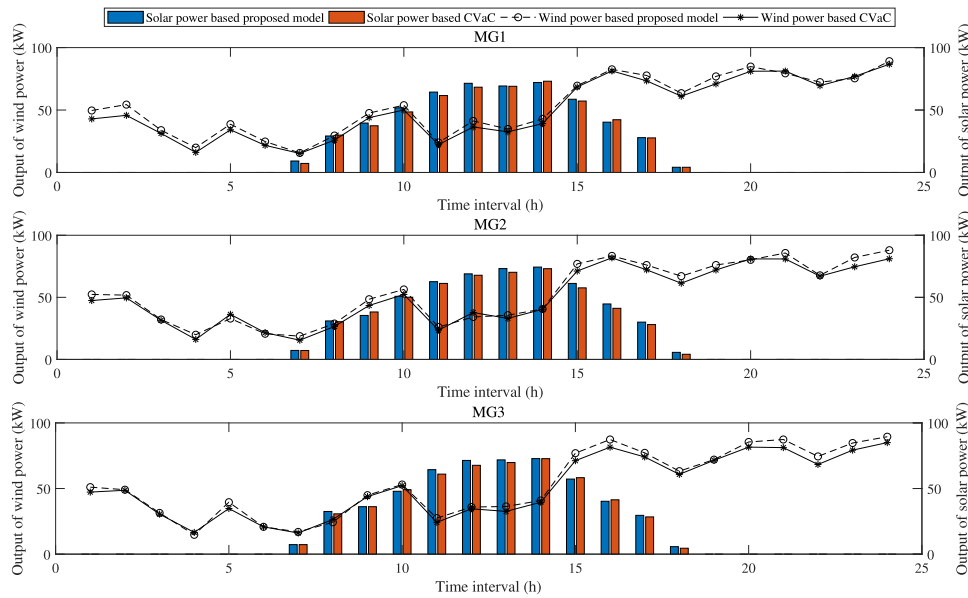
Fig. 10. Outputs of wind and solar power based on the proposed and CVaC model.

Table 7
The characteristics of the load curve in interconnected and unconnected MMG system.

Item	MG1			MG2			MG3		
	F1	F2	F3	F1	F2	F3	F1	F2	F3
Unconnected System	70.07%	61.69%	–	61.49%	92.61%	–	6.17%	187.89%	–
Interconnected System	**72.38**% ↑	**59.24**% ↓	0.43%	**63.69**% ↑	**82.19**% ↓	1.31%	**6.50**% ↑	**171.88**% ↓	8.12%

Table 8
Comparison of simulation results obtained by PSO, GSO and EPPS.

Algorithm	Maximum value ($)	Minimum value ($)	Mean value ($)	Standard deviation
PSO	1487.5647	1479.9278	1483.6825	2.6398
GSO	1480.1912	1472.2416	1475.1692	2.1142
EPPS	1477.8911	1471.4048	1474.2871	1.9316

times. By comparison, EPNS and EPC-based RA model can improve the penetration level of wind and solar power, which in turn the curtailed wind and solar is lower. In other words, BPIO and CVaC model are conservative for addressing the uncertainty of wind and solar power.

6.2.4. Simulation about algorithm comparison among PSO, GSO and EPPS
In order to verify the effectiveness of EPPS algorithm, we focus on comparing the performance of PSO, GSO and EPPS in terms of objective function value and convergence rate. Each algorithm runs independently for 30 times and the maximum number of calculations is set to 100,000. The simulation results are shown in Table 8. According to the comparison of maximum, minimum, mean, and standard deviation values, EPPS yields the best statistical properties. In addition, the convergence curves obtained by PSO, GSO and EPPS are provided in Fig. 11. From the figure, we can see that EPPS shows a faster convergence rate and a smaller accuracy.

The iteration will be stopped when the difference of the fitness values in two adjacent generations reaches an acceptable accuracy 1×10^{-3} or the function evaluation reaches the maximum number of iterations 100,000. From Fig. 11, we can see that algorithm reaches optimal solution after the approximately 55,000th iteration, and the difference between the two adjacent generations is 0.

7. Conclusions

This paper presents the MESS and power transaction-based flexibility enhancement strategy in MMG system, which aims to minimize the

MMG operating cost while mitigating the fluctuation of the net load with high penetrations of wind and solar power. Firstly, the temporal–spatial model of MESS is systematically designed to achieve charging/discharging service for MG. This approach guarantees that MESS is with good performance in dealing with the volatility and intermittence of wind and solar power. Then, the optimal MMG scheduling solution becomes feasible under EPNS and EPC-based RA model. Additionally, the EC problem of proposed model is formulated as a single-objective optimization problem and solved by EPPS algorithm.

We evaluated the performance of the proposed method on a three-microgrid system. MESS for MMG operation enables the reduction in operational cost of DG in each MG by 30.57%, 21.42% and 15.21%, the improvement in grid connection volumes of wind and solar in each MG by 10.01%, 6.03% and 3.81%, and the improvement in smoothness of the load curve in each MG by 1.22%, 1.36% and 0.26%, respectively. The results show that MESS for MMG operation can efficiently reduce the MMG operating cost, improve penetration level of wind and solar power as well as smooth load profile. Interconnected system for MMG operation enables the improvement in grid connection volumes of wind and solar in each MG by 9.60%, 5.15% and 4.10%, and the improvement in smoothness of the load curve in each MG by 2.31%, 2.20% and 0.33% in comparison with the unconnected system, respectively. The results show that interconnected system for MMG operation can efficiently improve penetration level of wind and solar power as well as smooth load profile. Additionally, EPNS and EPC-based RA can be well used as the risk measure for wind and solar uncertainty. In
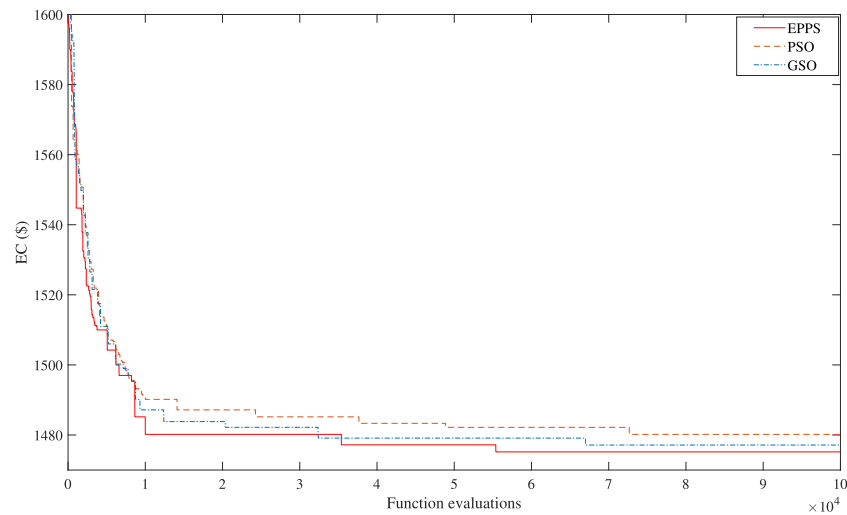
Fig. 11. Convergence curves of PSO, GSO and EPPS.

summary, this paper provides valuable experience for MMG operation by implementing MESS and power transaction.

CRediT authorship contribution statement

Z.L. Qu: Conceptualization, Data curation, Formal analysis, Funding acquisition, Investigation, Methodology, Project administration, Resources, Software, Supervision, Validation, Visualization, Writing - original draft, Writing - review & editing. **J.J. Chen:** Conceptualization, Data curation, Formal analysis, Investigation, Methodology, Resources, Visualization, Writing - original draft, Writing - review & editing. **K. Peng:** Conceptualization, Data curation, Formal analysis, Funding acquisition, Methodology, Project administration, Software, Supervision, Validation, Visualization, Writing - review & editing. **Y.L. Zhao:** Data curation, Formal analysis, Visualization, Writing - review & editing. **Z.K. Rong:** Data curation, Formal analysis, Writing - review & editing. **M.Y. Zhang:** Writing review & editing.

Declaration of competing interest

The authors declare that they have no known competing financial interests or personal relationships that could have appeared to influence the work reported in this paper.

References

Abdeltawab, H. H., & Mohamed, Y. A.-R. I. (2017). Mobile energy storage scheduling and operation in active distribution systems. *IEEE Transactions on Industrial Electronics, 64*(9), 6828–6840.

Al-Ghussain, L., Samu, R., Taylan, O., & Fahrioglu, M. (2020). Sizing renewable energy systems with energy storage systems in microgrids for maximum cost-efficient utilization of renewable energy resources. *Sustainable Cities and Society, 55,* Article 102059.

Amaris, H., Molina, Y. P., Alonso, M., & Luyo, J. E. (2018). Loss allocation in distribution networks based on Aumann–Shapley. *IEEE Transactions on Power Systems, 33*(6), 6655–6666.

Atia, R., & Yamada, N. (2016). Sizing and analysis of renewable energy and battery systems in residential microgrids. *IEEE Transactions on Smart Grid, 7*(3), 1204–1213.

Cagnano, A., De Tuglie, E., & Mancarella, P. (2020). Microgrids: Overview and guidelines for practical implementations and operation. *Applied Energy, 258,* Article 114039.

Chen, J. J., Wu, Q. H., Ji, T. Y., Wu, P. Z., & Li, M. S. (2016). Evolutionary predator and prey strategy for global optimization. *Information Sciences, 327,* 217–232.

Chen, J., Zhao, Y., Peng, K., & Wu, P. (2017). Optimal trade-off planning for wind-solar power day-ahead scheduling under uncertainties. *Energy, 141,* 1969–1981.

Croce, D., Giuliano, F., Bonomolo, M., Leone, G., Musca, R., & Tinnirello, I. (2020). A decentralized load control architecture for smart energy consumption in small islands. *Sustainable Cities and Society, 53,* Article 101902.

Cui, S., Wang, Y.-W., Shi, Y., & Xiao, J.-W. (2019). An efficient peer-to-peer energy-sharing framework for numerous community prosumers. *IEEE Transactions on Industrial Informatics, 16*(12), 7402–7412.

Das, B. K., Tushar, M. S. H., & Hassan, R. (2021). Techno-economic optimisation of stand-alone hybrid renewable energy systems for concurrently meeting electric and thermal loads. *Sustainable Cities and Society, 68,* Article 102763.

Dehnavi, E., & Abdi, H. (2016). Optimal pricing in time of use demand response by integrating with dynamic economic dispatch problem. *Energy, 109,* 1086–1094.

Elkadeem, M., Wang, S., Azmy, A. M., Atiya, E. G., Ullah, Z., & Sharshir, S. W. (2020). A systematic decision-making approach for planning and assessment of hybrid renewable energy-based microgrid with techno-economic optimization: A case study on an urban community in Egypt. *Sustainable Cities and Society, 54,* Article 102013.

Faria, E., Barroso, L. A., Kelman, R., Granville, S., & Pereira, M. V. (2009). Allocation of firm-energy rights among hydro plants: An aumann–shapley approach. *IEEE Transactions on Power Systems, 24*(2), 541–551.

Feng, W., Jin, M., Liu, X., Bao, Y., Marnay, C., Yao, C., & Yu, J. (2018). A review of microgrid development in the United States: A decade of progress on policies, demonstrations, controls, and software tools. *Applied Energy, 228,* 1656–1668.

Junqueira, M., da Costa, L. C., Barroso, L. A., Oliveira, G. C., Thomé, L. M., & Pereira, M. V. (2007). An Aumann–Shapley approach to allocate transmission service cost among network users in electricity markets. *IEEE Transactions on Power Systems, 22*(4), 1532–1546.

Kim, J., & Dvorkin, Y. (2018). Enhancing distribution system resilience with mobile energy storage and microgrids. *IEEE Transactions on Smart Grid, 10*(5), 4996–5006.

Kwon, S.-Y., Park, J.-Y., & Kim, Y.-J. (2019). Optimal V2G and route scheduling of mobile energy storage devices using a linear transit model to reduce electricity and transportation energy losses. *IEEE Transactions on Industry Applications, 56*(1), 34–47.

Lei, S., Wang, J., Chen, C., & Hou, Y. (2016). Mobile emergency generator pre-positioning and real-time allocation for resilient response to natural disasters. *IEEE Transactions on Smart Grid, 9*(3), 2030–2041.

Li, Y., Li, K., Wang, P., Liu, Y., Lin, X., Gooi, H., Li, G., Cai, D., & Luo, Y. (2017). Risk constrained economic dispatch with integration of wind power by multi-objective optimization approach. *Energy, 126,* 810–820.

Li, Y. Z., Wu, Q. H., Li, M. S., & Zhan, J. P. (2014). Mean-variance model for power system economic dispatch with wind power integrated. *Energy, 72,* 510–520.

Li, Y., Zhao, T., Wang, P., Gooi, H. B., Wu, L., Liu, Y., & Ye, J. (2018). Optimal operation of multimicrogrids via cooperative energy and reserve scheduling. *IEEE Transactions on Industrial Informatics, 14*(8), 3459–3468.

Liu, Z., Zhang, Z., Zhuo, R., & Wang, X. (2019). Optimal operation of independent regional power grid with multiple wind-solar-hydro-battery power. *Applied Energy, 235,* 1541–1550.

Paul, S., Nath, A. P., & Rather, Z. H. (2019). A multi-objective planning framework for coordinated generation from offshore wind farm and battery energy storage system. *IEEE Transactions on Sustainable Energy, 11*(4), 2087–2097.

Ran, X., Miao, S., Jiang, Z., & Xu, H. (2015). A framework for uncertainty quantification and economic dispatch model with wind–solar energy. *International Journal of Electrical Power & Energy Systems, 73*, 23–33.

Ruan, H., Gao, H., Liu, Y., Wang, L., & Liu, J. (2020). Distributed voltage control in active distribution network considering renewable energy: A novel network partitioning method. *IEEE Transactions on Power Systems, 35*(6), 4220–4231.

Ustun, T. S., Ozansoy, C., & Zayegh, A. (2011). Recent developments in microgrids and example cases around the world: A review. *Renewable & Sustainable Energy Reviews, 15*(8), 4030–4041.

Wang, Y., Huang, Z., Shahidehpour, M., Lai, L. L., Wang, Z., & Zhu, Q. (2019). Reconfigurable distribution network for managing transactive energy in a multi-microgrid system. *IEEE Transactions on Smart Grid, 11*(2), 1286–1295.

Wu, L., Shahidehpour, M., & Li, Z. (2012). Comparison of scenario-based and interval optimization approaches to stochastic SCUC. *IEEE Transactions on Power Systems, 27*(2), 913–921.

Yao, S., Wang, P., & Zhao, T. (2019). Transportable energy storage for more resilient distribution systems with multiple microgrids. *IEEE Transactions on Smart Grid, 10*, 3331–3341.

Zhang, B., Li, Q., Wang, L., & Feng, W. (2018). Robust optimization for energy transactions in multi-microgrids under uncertainty. *Applied Energy, 217*, 346–360.

Zhao, B., Chen, J., Zhang, L., Zhang, X., Qin, R., & Lin, X. (2018). Three representative island microgrids in the East China Sea: Key technologies and experiences. *Renewable & Sustainable Energy Reviews, 96*, 262–274.

Zheng, Y., Meng, K., Luo, F., Qiu, J., & Zhao, J. (2018). Optimal integration of MBESSs/SBESSs in distribution systems with renewables. *IET Renewable Power Generation, 12*(10), 1172–1179.